UCLA
COMPUTATIONAL AND APPLIED MATHEMATICS

Convex ENO High Order Multi-dimensional Schemes Without Field by Field Decomposition or Staggered Grids

Xu-Dong Liu
Stanley Osher

June 1997

CAM Report 97-26

Department of Mathematics
University of California, Los Angeles
Los Angeles, CA. 90095-1555

Convex ENO High Order Multi-dimensional Schemes Without Field by Field Decomposition or Staggered Grids

Xu-Dong Liu * Stanley Osher†

Running head: Convex ENO Schemes

Proofs sent to:

Xu-Dong Liu

Department of Mathematics
UCSB
Santa Barbara, CA 93106

AMS(MUS) subject classification: Primary 65M10; Secondary 65M05

Keywords: Multi-dimensional Systems of Conservation Laws, High Order Accurate Convex ENO Schemes.

*Dept of Math, UCSB, Santa Barbara, CA 93106 xliu@math.ucsb.edu
†Dept of Math, UCLA, Los Angeles, CA 90095, sjo@math.ucla.edu, Research supported by DARPA URI ONR-N00014-92-J-1890, NSF DMS94-04942 and ARO DAAH04-95-I-0155

Abstract

Second order accurate (first order at extrema) cell averaged based approximations extending the Lax-Friedrichs central scheme, using component-wise rather than field-by-field limiting, have been found to give surprisingly good results for a wide class of problems involving shocks [15]. The advantages of component-wise limiting compared to its counterpart, field-by-field limiting, are apparent: (1) No complete set of eigenvectors is needed and hence weakly hyperbolic systems can be solved. (2) Component-wise limiting is faster than field-by-field limiting. (3) The programming is much simpler, especially for complicated coupled systems of many equations. However these methods are based on cell-averages in a staggered grid and are thus a bit complicated to extend to multiple dimensions. Moreover the staggering causes slight difficulties at the boundaries.

In this work we modify and extend this component-wise central differencing based procedure in two directions: (1) Point values, rather than cell averages are used, thus removing the need for staggered grids, and also making the extension to multi-dimensions quite simple. We use TVD Runge-Kutta time discretizations to update the solution. (2) A new type of decision process, which follows the general ENO philosophy is introduced and used. This procedure enables us to extend our method to a third order component-wise central ENO scheme, which apparently works well and is quite simple to implement in multi-dimensions. Additionally, our numerical viscosity is governed by the local magnitude of the maximum eigenvalue of the Jacobian, thus reducing the smearing in the numerical results. We found a speed up of a factor of 2 in each space dimension, on a SGI O_2 workstation, over methods based on field-by-field decomposition limiting.

The new decision process leads to new, "convex" ENO schemes which, we believe, are of interest in a more general setting.

Our numerical results show the value of these new methods.

1 Introduction

Essentially Non-Oscillatory (ENO) schemes as developed in [6] and modified in [19] form a general method for solving systems of hyperbolic conservation laws in several space dimensions. The goal is high order accuracy in smooth regions, without significant spurious oscillations near jumps, done within a conservation form setting. The original method as developed in [6] used the natural cell average based formulation. This was modified in [19] using a conservation form approximation to point values, and was implemented dimension by dimension (*not* by dimensional splitting). The original method advocated a rather complicated time discretization based on replacing time derivatives by space derivatives. The modification in [19] used any of a class of simple TVD Runge-Kutta time discretizations, developed for that purpose in [18], thus separating out the space and time derivatives.

The most intimidating and expensive part of ENO (and other high resolution methods such as 2nd order TVD) is the field-by-field decomposition in which the Jacobian matrices are somehow diagonalized locally, interpolation (or limiting) is done in each eigenspace and the numerical fluxes are reassembled out of these components. In [6] the field-by-field decomposition was strongly advocated. Significant oscillations were obtained in a test example Riemann problem which used component-wise reconstructions.

The advantages of component-wise limiting compared to its counterpart, field-by-field limiting, are apparent: (1) No complete set of eigenvectors is needed and hence weakly hyperbolic systems can be solved. (2) Component-wise limiting is faster than field-by-field limiting (In our numerical tests we found that component-wise limiting is 2 times faster than field-by-field limiting in *each* dimension). (3) The programming is much simpler for complicated coupled systems of many equations. In [15, 10] second order accurate (first order at extrema) sequels to the canonical first-order central difference scheme, the Lax-Friedrichs scheme, using component wise limiting were found to give surprisingly good results. The oscillations were typically $O(1)$, but very small. These methods were based on a cell average on a staggered grid and were, therefore, a bit complicated to extend to two space dimensions. Moreover boundary conditions posed a slight difficulty due to the staggering. A third order cell average based scheme of this type, using a non-oscillatory reconstruction from [12] was obtained in [13]. We also note that the relaxing method in [11] is close to the second order accurate component-wise scheme in [15].

Drawing on the above authors' very positive experience with component-wise central high resolution schemes based on cell averages, we attempt here to modify and extend this procedure in two directions. (1) Point values rather than cell averages are used, thus removing the need for staggered grids and making the extension to multi-dimensions quite simple via the TVD Runge-Kutta time discretization. (2) A new type of decision within the ENO philosophy

is introduced and used below. This enables us to extend our pointwise second order central scheme to a third order component-wise central essentially non-oscillatory scheme which apparently works well and is simple to implement in multi-dimensions. Of course this new type of decision also works well under a field-by-field decomposition framework. Additionally, our numerical viscosity may be governed by the local magnitude of the maximum eigenvalue determined locally. Thus, our schemes should have the smallest possible viscosity within this central scheme framework. We note that H. Choi and J. Liu [2] have also used component-wise limiting in a flux-split second order context. Our schemes differ from theirs as follows: (1) We proceed to third order accurate methods using the convex ENO idea presented in section III below. (2) Their interesting and new limiting procedure is such that their flux does not degenerate to a formally first order accurate method at discontinuities for their (second order) method. Ours does, and this accounts for our less oscillatory results, even for our third order method.

The format of this paper is as follows. In the next section we describe the very simple new second order (perhaps first order at extrema) component-wise point value scheme. In section III we describe our new ENO like decision process and then use it to devise our third order accurate essentially non-oscillatory component-wise central scheme. We call this decision process convex ENO. We expect this idea to be useful elsewhere. Finally, in section IV, we present numerical examples showing the utility of our new and simple methods for both component-wise and field-by-field decomposition implementations.

We believe that a component-wise scheme will perform well only if the flux is close to that of a field-by-field scheme. Of course, in regions of smoothness, formal truncation error analysis implies that this is true. However, near discontinuities, the flux must be close to a flux which does not mix the fields. Our convex ENO philosophy – stay as close as possible to a second order TVD (or UNO) flux which degenerates to first order at discontinuities, while maintaining formal higher order accuracy – is designed to do this.

Acknowledgment: We would like to thank R. Fedkiw, G.-S. Jiang, B. Merriman and E. Tadmor for valuable discussions on this topic. In particular we thank Professor Tadmor for insisting that the automatic degeneracy to first order accuracy in the flux for second order component-wise schemes was a key to their success.

2 A Second Order Accurate Multidimensional High Resolution Scheme Without Field-by-Field Decompositions or Staggered Grids

We follow the derivation in [19] with one major and obvious change, which is quite significant (see the acknowledgment) in the absence of the field-by-field decomposition.

Our set up is as follows.

We shall solve the hyperbolic system of conservation laws

$$(1) \qquad \begin{cases} q_t + \sum_{i=1}^{d} f_i(q)_{x_i} = 0 \quad (\text{or } g(u,x,t), \text{ a forcing term}) \\ q(x,0) = q_0(x). \end{cases}$$

Here $q = (q, \ldots, q_n)^T$, $x = (x^1, \ldots, x^d)$, and any real linear combination of the Jacobian matrices $\sum_{i=1}^{d} \xi_i \left(\frac{\partial f_i}{\partial q}\right)$ has only real eigenvalues.

The first and second order accurate schemes used below all have the usual theoretical justification in the scalar case. Namely the first order schemes based on monotone or E scheme building blocks converge in multi-dimensions to the correct entropy satisfying solution. The second order TVD based schemes satisfy a maximum principle in multi-dimensions and are variation non-increasing in one dimension (except when the "UNO" limiter of [7] is used – then we are only assured that the number of extrema is non-increasing). The proofs are routine by now and omitted here – see e.g. [16, 7] and the references therein. The third and higher order ENO based schemes have no rigorous theory but work well in practice [6, 19]. Finally we note that the entropy condition can be proven easily for the first order versions for systems of equations which admit a convex entropy.

On the computational grid: $x_j = j\Delta x$, $t_n = n\Delta t$, we use q_j^n to denote the computed approximation to the exact solution $q(x_j, t_n)$.

We begin our discussion with the one space dimension, scalar case.

We shall always use conservative schemes of the form

$$q_j^{n+1} = q_j^n - \lambda(\hat{f}_{j+\frac{1}{2}} - \hat{f}_{j-\frac{1}{2}}), \quad \lambda = \frac{\Delta t}{\Delta x} \tag{2}$$

with a consistent numerical flux

$$\hat{f}_{j+\frac{1}{2}} = \hat{f}(q_{j-l}, \ldots, q_{j+k}), \quad \hat{f}(q, \ldots, q) = f(q). \tag{3}$$

We start with a simple first order monotone Lax-Friedrich type of central scheme, as in [19]. We define

$$f^+(q) = \frac{1}{2}(f(q) + \alpha q), \; f^-(q) = \frac{1}{2}(f(q) - \alpha q) \tag{4}$$

where $\alpha \geq \max |f'(q)|$. We have

$$f^{+'}(q) \geq 0, \; f^{-'}(q) \leq 0 \tag{5}$$

$$f^+(q) + f^-(q) = f(q). \tag{6}$$

The Lax-Friedrichs scheme is simply (2) with

$$\hat{f}^{LF}_{j+\frac{1}{2}} = f^+_j + f^-_{j+1} \tag{7}$$

where $f^+_j = f^+(q_j)$ and $f^-_{j+1} = f^-(q_{j+1})$.

Notice that the dissipation α is independent of Δt, (and does not blow up as $\Delta t \downarrow 0$) in contrast to the staggered grid version.

An alternative, less dissipative, type of central scheme is obtained by defining:

$$f^+_{j+\frac{1}{2}}(q) = \frac{1}{2}(f(q) + \alpha_{j+\frac{1}{2}} q), \qquad f^-_{j+\frac{1}{2}}(q) = \frac{1}{2}(f(q) - \alpha_{j+\frac{1}{2}} q) \tag{8}$$

where

$$\alpha_{j+\frac{1}{2}} = \max_{\min(q_j, q_{j+1}) \leq q \leq \max(q_j, q_{j+1})} |f'(q)| \tag{9}$$

and the analogue of (6) is valid.

Note, that if $f''(q) \neq 0$, on the interval above, then:

$$\alpha_{j+\frac{1}{2}} = \max(|f'(q_j)|, |f'(q_{j+1})|). \tag{10}$$

The local Lax-Friedrichs scheme is defined to be (2) with

$$\hat{f}^{LLF}_{j+\frac{1}{2}} = f^+_{j+\frac{1}{2}}(q_j) + f^-_{j+\frac{1}{2}}(q_{j+1}). \tag{11}$$

This is also a monotone scheme [19].

Clearly, other possible candidates for $\alpha_{j+1/2}$ exist – one might search in a full multidimensional interval and use the maximum eigenvalues of the corresponding Jacobian matrices to estimate the viscosity coefficient – see e.g. [14].

Next we review and modify our procedure for constructing second order ENO schemes.

As defined in [19], (algorithm 2.2, $r = 1$) the numerical flux corresponding to each of $f^{\pm}(q)$ comes from differentiating a quadratic interpolant of the primitive function (again see [19]). The interpolant is chosen to be the one which has the smaller (in magnitude) second derivative of two candidates. The (ENO) motivation for this choice was that choosing one or the other enables us to proceed to a higher degree polynomial, hence higher order accurate flux, in an hierarchical fashion. If we stop at a second order accurate level, then although this decision results (for scalars) in a non-oscillatory, in fact, TVD scheme, it leads to problems (oscillations) when used in a component-wise fashion. The main problem is that the numerical flux does *not* degenerate to the associated first order flux $\hat{f}^{LLF}_{j+\frac{1}{2}}$;

at discontinuities. Thus fields do mix, unlike in the first order Lax-Friedrichs case. This leads us to a (trivial to implement) change in the flux for our second order accurate method.

The standard second order ENO LLF flux is defined by

$$
\begin{aligned}
\hat{f}^{LLF,2}_{j+\frac{1}{2}} &= \tfrac{1}{2}(f(q_{j+1}) + f(q_j) - \alpha_{j+\frac{1}{2}}(q_{j+1} - q_j)) \\
&+\tfrac{1}{4}m[\Delta_+ f(q_j) + \alpha_{j+\frac{1}{2}}\Delta_+ q_j,\ \Delta_- f(q_j) + \alpha_{j+\frac{1}{2}}\Delta_- q_j] \\
&-\tfrac{1}{4}m[\Delta_+ f(q_{j+1}) - \alpha_{j+\frac{1}{2}}\Delta_+ q_{j+1}, \Delta_- f(q_{j+1}) - \alpha_{j+\frac{1}{2}}\Delta_- q_{j+1}]
\end{aligned} \tag{12}
$$

where

$$
\Delta_\pm p_j = \pm(p_{j\pm1} - p_j) \tag{13}
$$

and

$$
m(x,y) = \begin{cases} x & \text{if } |x| \le |y| \\ y & \text{otherwise} \end{cases} \tag{14}
$$

The usual second order TVD flux is exactly the same as (12) except that we replace m by a Lipschitz continuous function which degenerates to zero when the two arguments are of opposite sign. See e.g. [20] for an analysis of these (classical) TVD limiters.

The canonical example is the minmod limiter:

$$
mm(x,y) = \begin{cases} (\text{sign } x)\min(|x|,|y|) & \text{if } xy > 0 \\ 0 & \text{otherwise.} \end{cases} \tag{15}
$$

An alternative way of writing the flux with general limiters following the notation of [20] is

$$
\begin{aligned}
\hat{f}^{LLf,2}_{j+\frac{1}{2}} &= \tfrac{1}{2}(f(q_{j+1}) + f(q_j) - \alpha_{j+\frac{1}{2}}(q_{j+1} - q_j)) \\
&+\tfrac{1}{4}[\varphi(r^+_j)(\Delta_+ f(q_j) + \alpha_{j+\frac{1}{2}}\Delta_+ q_j) - \varphi(r^-_{j+1})(\Delta_+ f(q_{j+1}) - \alpha_{j+\frac{1}{2}}\Delta_+ q_{j+1})]
\end{aligned} \tag{16}
$$

where

$$
r^+_j = \frac{(\Delta_- f(q_j) + \alpha_{j+\frac{1}{2}}\Delta_- q_j)}{(\Delta_+ f(q_j) + \alpha_{j+\frac{1}{2}}\Delta_+ q_j)} \tag{17}
$$

$$
r^-_{j+1} = \frac{(\Delta_- f(q_{j+1}) - \alpha_{j+\frac{1}{2}}\Delta_- q_{j+1})}{(\Delta_+ f(q_{j+1}) - \alpha_{j-\frac{1}{2}}\Delta_+ q_{j+1})}. \tag{18}
$$

For the limiter m defined in (4) we have

$$
\varphi_m(r) = \begin{cases} 1 & \text{if } 1 \le |r| \\ r & \text{otherwise} \end{cases} \tag{19}
$$

This limiter does not vanish if $r < 0$; this (together with the discontinuity at $r = -1$) proves disastrous in the absence of field-by-field limiting.

The scheme using mm corresponds to

$$
\varphi_{mm}(r) = \max(0, \min(r, 1)). \tag{20}
$$

This is the least compressive, most smearing, and most reliable limiter (least likely to induce oscillations in a component-wise framework).

The most compressive TVD limiter, due to P. Roe is called superbee and corresponds to

$$
\varphi_{sb}(r) = \max(0, \min(2r, 1), \min(r, 2)). \tag{21}
$$

Finally, a very good compromise between these two is due to van Leer

$$
\varphi_{VL}(r) = \frac{r + |r|}{1 + |r|}. \tag{22}
$$

All of the schemes corresponding to these φ are second order TVD and hence degenerate to first order at smooth extrema (and discontinuities, of course).

Harten and Osher began their construction of ENO schemes in [7], replacing the TVD condition with the uniformly non-oscillatory (UNO) notion – the *number* of extrema is non increasing. The resulting scheme involves minmods, so it degenerates to first order accuracy at discontinuities, but not at smooth extrema. In the present context, the flux using the UNO limiter is:

$$\begin{aligned} f^{LLF,2}_{j+\frac{1}{2}} &= \tfrac{1}{2}(f(q_{j+1}) + f(q_j) - \alpha_{j+\frac{1}{2}}(q_{j+1} - q_j)) \\ +\tfrac{1}{4}mm[&\Delta_+ f(q_j) + \alpha_{j+\frac{1}{2}}\Delta_+ q_j - \tfrac{1}{2}mm[\Delta_+\Delta_- f(q_j) + \alpha_{j+\frac{1}{2}}\Delta_+\Delta_- q_j, \Delta_+\Delta_- f(q_{j+1}) + \alpha_{j+\frac{1}{2}}\Delta_+\Delta_- q_{j+1}], \\ &\Delta_- f(q_j) + \alpha_{j+\frac{1}{2}}\Delta_- q_j + \tfrac{1}{2}mm[\Delta_+\Delta_- f(q_{j-1}) + \alpha_{j+\frac{1}{2}}\Delta_+\Delta_- q_{j-1}, \Delta_+\Delta_- f(q_j) + \alpha_{j+\frac{1}{2}}\Delta_+\Delta_- q_j]] \\ -\tfrac{1}{4}mm[&\Delta_+ f(q_{j+1}) - \alpha_{j+\frac{1}{2}}\Delta_+ q_{j+1} - \tfrac{1}{2}mm[\Delta_+\Delta_- f(q_{j+1}) - \alpha_{j+\frac{1}{2}}\Delta_+\Delta_- q_{j+1}, \Delta_+\Delta_- f(q_{j+2}) - \alpha_{j+\frac{1}{2}}\Delta_+\Delta_- q_{j+2}], \\ &\Delta_- f(q_{j+1}) - \alpha_{j+\frac{1}{2}}\Delta_- q_{j+1} + \tfrac{1}{2}mm[\Delta_+\Delta_- f(q_j) - \alpha_{j+\frac{1}{2}}\Delta_+\Delta_- q_j, \Delta_+\Delta_- f(q_{j+1}) - \alpha_{j+\frac{1}{2}}\Delta_+\Delta_- q_{j+1}]] \end{aligned} \tag{23}$$

The second order accurate fluxes corresponding to the LF scheme are denoted as $\hat{f}^{LF,2}_{j+1/2}$ (differing from LLF only in the replacement of $\alpha_{j+1/2}$ by a fixed sufficiently large constant). We denote the flux by using the limiter and the choice LLF or LF as follows:

$$\hat{f}^{LLF,mm}_{j+1/2}, \quad \hat{f}^{LF,uno}_{j+1/2}. \tag{24}$$

Next we turn to systems of conservation laws. At this point the reader is usually advised to compute eigenvalues and left and right eigenvectors of the Jacobian matrix at some intermediate point. Instead, we need only an upper bound of the magnitude of the largest eigenvalue, either for all q in the range of values taken on at a given time level, (for LF), or for all q such that each component lies in the range of values between the components of q_j, and q_{j+1} (for LLF).

Then our scheme is easily constructed. Having picked the constant $\alpha_{j+1/2}$, we simply interpret all of our flux formulae (16)-(24) component by component with the *same* $\alpha_{j+1/2}$ for each component.

Thus we have constructed our flux for systems of conservation laws in one dimension. For multi-dimensions, we simply do the same thing component-wise for each of the f_i in (1).

We may now proceed in either of two ways:

(A) For a second order accurate method we denote our approximation by

$$\sum_{i=1}^{d}(f_i(q))_{x_i} = -(\mathcal{L}_\Delta(q)). \tag{25}$$

Then we use the two step TVD *RK* method (which is just the classical Heun's method) to update this:

$$\begin{aligned} q^{(1)} &= q^n + \Delta t\mathcal{L}_\Delta(q^n) \\ q^{n+1} &= \tfrac{1}{2}(q^{(1)} + q^n) + \tfrac{\Delta t}{2}\mathcal{L}_\Delta(q^{(1)}). \end{aligned} \tag{26}$$

(B) For a third order accurate method we use each component of our second order accurate flux, constructed above together with a new ENO like decision, to help construct a simple third order accurate approximation which we again call $-(\mathcal{L}_\Delta(q))$. Then we use the simple three step TVD *RK* method developed in [18] to update this in time – see equation (34) in the next section.

3 High Order accurate Multidimensional ENO Schemes Without Field-by-Field Decomposition or Staggered Grids, Using a Convex ENO Decision Process

We shall modify the standard ENO process in order to design our new third order scheme. The details of this modification as applied to the particular problem at hand may appear to be complicated, but the new idea is quite

simple. To create a higher order accurate, essentially non-oscillatory approximation to a function and sample this approximation or some derivative of it, proceed hierarchically. Start with a linear approximation. Next take the usual two candidate quadratic approximations, sample each, take the convex combination of the two samples which is closest to the linear sample. Then proceed hierarchically.

In the present case, the rules are as follows: Given values of a function $H(x)$ at lattice points $x = x_k$, we wish to get a high order non-oscillatory approximation to $H'(x)$ at $x = x_j$. We start with a linear interpolant at stencil (x_{j-1}, x_j). (This is connected with the construction of an approximation to f^+; the construction for f^- starts with (x_j, x_{j+1}). Differentiating this interpolant leads us to the first order approximation

$$H^{(1)'}(x_j) \approx \frac{H(x_j) - H(x_{j-1})}{\Delta x} = I^{(1)'}_{j-1,j}(x_j). \tag{27}$$

To proceed and obtain a second order approximation, we consider two quadratic interpolants which use (x_{j-2}, x_{j-1}, x_j) and (x_{j-1}, x_j, x_{j+1}) respectively. By differentiating these two polynomials we get two candidates for the approximation.

$$H^{(2)'}(x_j) \approx I^{(2)'}_{j-2,j} = \frac{H(x_j) - H(x_{j-1})}{\Delta x} - \frac{1}{2}\left(\frac{H(x_j) - 2H(x_{j-1}) + H(x_{j-2})}{\Delta x}\right) \tag{28}$$

$$H^{(2)'}(x_j) \approx I^{(2)'}_{j-1,j+1}(x_j) = \frac{H(x_j) - H(x_{j-1})}{\Delta x} - \frac{1}{2}\left(\frac{(H(x_{j+1}) - 2H(x_j) + H(x_{j-1})}{\Delta x}\right). \tag{29}$$

The normal ENO decision would be to choose the "smoother" of the two. All the other limiter type decisions would involve picking one of the above, or degenerating to first order (at extrema or discontinuities). We propose the following, which is generally slightly different: Take the convex combination of $I^{(2)'}_{j-1,j+1}(x_j), I^{(2)'}_{j,j+2}(x_j)$ which is closest to $I^{(1)'}_{j-1,j}(x_j)$, the "monotone" approximation. Interestingly enough, this reduces to the min mod decision in this case, and generalizes it at a higher order level

$$H^{(2)'}(x_j) = \frac{\Delta_- H(x_j)}{\Delta x} - \frac{1}{2\Delta x} mm[\Delta_-\Delta_- H(x_j), \Delta_+\Delta_- H(x_j)]. \tag{30}$$

Thus, we have nothing really new here. However, we go to higher order by storing this choice and proceeding.

For third order, we select three cubic interpolants of H at stencils $(x_{j-3}, x_{j-2}, x_{j-1}, x_j)$, $(x_{j-2}, x_{j-1}, x_j, x_{j+2})$, and $(x_{j-1}, x_j, x_{j+1}, x_{j+2})$, differentiate each of the interpolants, then evaluate the results at x_j, and take the convex combination of these numbers which is "closest" to $H^{(2)'}(x_j)$. This gives us $H^{(3)'}(x_j)$. The "closest" is explained in the next paragraph.

Inductively: given an $(n-1)^{\text{st}}$ order approximation $H^{(n-1)'}(x_j)$, we take n n^{th} order interpolants of $H(x)$, using $(x_{j-n}, \ldots, x_j), (x_{j-n+1}, \ldots, x_{j+1}) \cdots (x_{j-1}, \ldots, x_{j+n-1})$. We get n candidates for $H^{(n)'}(x_j)$. Denote them by $H^{(n)'}_\nu(x_j)$, $\nu = 1, \ldots, n$. Our procedure is to take the convex combination of these n candidates which is "closest" to $H^{(n-1)'}(x_j)$ in the following sense:

Convex ENO:

$$\begin{array}{llll} \text{(step 1)} & \text{Calculating} & d_\nu = \alpha_\nu(H^{(n)'}_\nu(x_j) - H^{(n-1)'}(x_j)) & \text{for }, \nu = 1, \ldots, n \\ \text{(step 2)} & \text{If} & sign(d_\nu) \text{ are different,} & \text{then } H^{(n)'}(x_j) = H^{(n-1)'}(x_j) \\ \text{(step 3)} & \text{Else if} & \mid d_{\nu_0} \mid \leq \min_{1 \leq \nu \leq n} \mid d_\nu \mid & \text{then } H^{(n)'}(x_j) = H^{(n)'}_{\nu_0}(x_j) \end{array} \tag{31}$$

where $0 \leq \alpha_\nu \leq 1, \nu = 1, \ldots, n$ are chosen to bias toward central interpolations to avoid the loss of accuracy, which is the same technique used in [17].

This inductive process is uniformly high order accurate, *maximally accurate*, yet degenerates to agree with a lower order interpolant when appropriate (near where the n^{th} derivative of H vanishes, or near its discontinuities).

Next we turn to our construction of high order ENO methods using this approximation procedure. Following [19], using our new hierarchical process, we easily can build up higher order schemes in the scalar case using LF or LLF building blocks. Extensions to systems and multi-dimensions are routine, as described in the previous section. In this work, we proceed as follows.

We begin with any of the second order accurate fluxes constructed in the previous section, e.g. $\hat{f}^{LLF,mm}_{j+1/2}, \hat{f}^{LF,uno}_{j+1/2}$, decomposed into its upwind (+) and downwind (-) components. We instruct a third order accurate flux by interpolating $H^+(x)$, see [19], at $(x_{j-1/2}, x_{j+1/2})$ and two more points. The three candidates involve $(x_{j-5/2}, x_{j-3/2}, x_{j-1/2}, x_{j+1/2})$, $(x_{j-3/2}, x_{j-1/2}, x_{j+1/2}, x_{j+3/2})$, $(x_{j-1/2}, x_{j+1/2}, x_{j+3/2}, x_{j+5/2})$. Construct the three cubic interpolants. The divided difference tables for $H^{\pm}$ can be obtained from those of f as in [19], eqn. (11a,b). We repeat the formulae here:

$$H^{\pm}[x_{\ell-\frac{1}{2}}, x_{\ell+\frac{1}{2}}] = \frac{1}{2}(f[u(x_\ell)] \pm \alpha_{j+\frac{1}{2}} u[x_\ell]) \tag{32}$$

$$H^{\pm}[x_{\ell-\frac{1}{2}}, \ldots, x_{\ell+k+\frac{1}{2}}] = \frac{1}{k+1} \cdot \frac{1}{2}(f[u(x_\ell), \ldots, u(x_{\ell+k})] \pm \alpha_{j+\frac{1}{2}} u[x_\ell, \ldots, x_{\ell+k}]) \tag{33}$$

where $H[x_\nu, \ldots, x_{\nu+k}]$ is the usual Newton coefficient.

Thus $(H^+)'(x_{j-\frac{1}{2}})$ is approximated by a convex combination of the three quantities gotten through this interpolating procedure. Again we take the closest convex combination to our $f^{+LLF,2}_{j+\frac{1}{2}}$ (or $f^{+LF,2}_{j+\frac{1}{2}}$, if $\alpha_{j+1/2}$ is a fixed constant independent of j).

We, of course, do the analogous thing for $(H^-)'(x_{j+\frac{1}{2}})$. Then we add the two approximations and get our flux: $f^{LLF,3}_{j+\frac{1}{2}}$ or $f^{LF,3}_{j+\frac{1}{2}}$. Here we chose $\alpha_1 = 1, \alpha_2 = 0.7, \alpha_3 = 1$ for component-wise convex ENO schemes; and $\alpha_1 = 1, \alpha_2 = 0.5, \alpha_3 = 1$ for field-by-field convex ENO schemes. This is similar to the weighting used in [17] to avoid the local loss of accuracy.

Systems are approximated component by component for these convex ENO schemes. Multidimensional problems are done dimension by dimension (*not by dimensional spitting*) and the third order accurate TVD space RK time discretization introduced in [19] is used. For completeness we present the time discretization algorithm, following the notation of (25):

$$\begin{aligned} q^{(1)} &= q^n + \Delta t \mathcal{L}_\Delta(q^n) \\ q^{(2)} &= \tfrac{3}{4}q^n + \tfrac{1}{4}q^{(1)} + \tfrac{1}{4}\Delta t \mathcal{L}(q^{(1)}) \\ q^{n+1} &= \tfrac{1}{3}q^n + \tfrac{2}{3}q^{(2)} + \tfrac{2}{3}\Delta t \mathcal{L}(q^{(2)}). \end{aligned} \tag{34}$$

This completes the construction of the third order accurate component-wise and field-by-field convex ENO schemes.

Clearly, we can construct higher order convex ENO based schemes this way. We shall investigate this in the future.

4 Numerical Results

All of our one dimensional problems are to be solved for $0 \le x \le 1$, $t > 0$. The first scheme tested is our 3rd order accurate component-wise convex ENO scheme using the minmod limiter at the second order step (unless we indicate a different choice of limiter). We call this the component-wise convex ENO scheme. The second scheme is our 3rd order accurate field-by-field convex ENO scheme for which we use the UNO limiter. We call this the field-by-field convex ENO scheme.

Example 1: We begin with a test problem due to Engquist (private communication)

$$U_t + AU_x = 0, \tag{35}$$

where $U = \begin{pmatrix} u_1 \\ u_2 \end{pmatrix}$ and $A = \begin{pmatrix} 0 & 1 \\ 1 & 0 \end{pmatrix}$.

Our initial data is

$$\begin{aligned} u_1(x,0) &\equiv 1, && 0 \le x \le 1 \\ u_2(x,0) &= \begin{cases} 1, & 0 \le x < 0.5 \\ 0, & 0.5 \le x < 1 \end{cases} \end{aligned} \tag{36}$$

We take periodic boundary conditions. In Figures 1a-1b we present the numerical results obtained by using our component-wise convex ENO scheme, first by using the minmod limiter at the second order step, second by using the superbee limiter at that step. Unsurprisingly, the superbee limiter gives somewhat sharper results, but the profiles are non-oscillatory (in the primitive variables) in both cases. However, we warn the reader that our results for the Euler equations of gas dynamics using the superbee based third order method are not satisfactory.

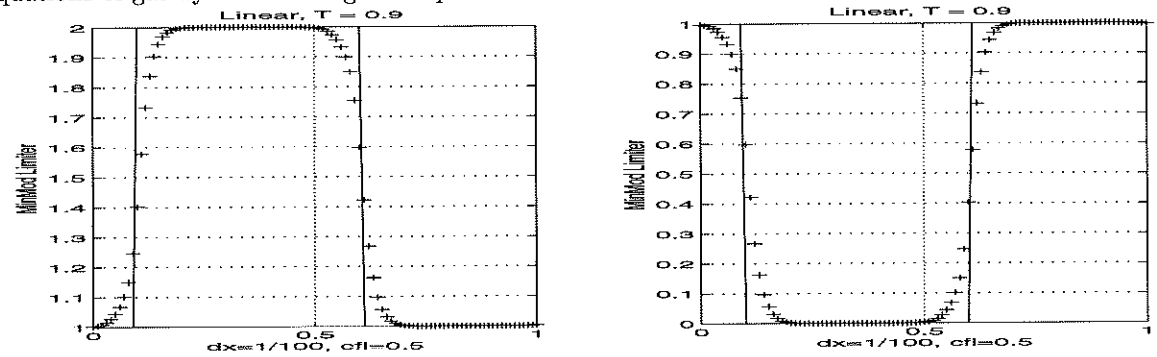

Figure 1a: 3rd order component-wise CENO, mimmod limiter, Engquist example

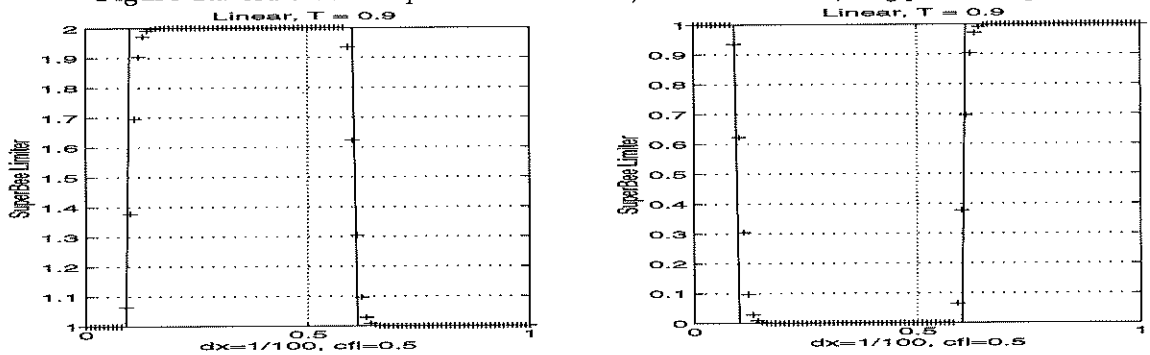

Figure 1b: 3rd order component-wise CENO, superbee limiter, Engquist example

Next we consider the one-dimensional Euler equations for a polytropic gas:

$$U_t + F(U)_x = 0,$$

where

(37)
$$U = \begin{pmatrix} \rho \\ m \\ E \end{pmatrix}, \quad F(U) = \begin{pmatrix} m \\ \rho u^2 + P \\ u(E+\rho) \end{pmatrix}$$

with

$$P = (\gamma - 1)(E - \frac{1}{2}\rho u^2)$$

and

$$m = \rho u$$

with $\gamma = 1.4$ for air.

We next consider six different initial value problems.

Example 2: Sod's Riemann problem: Initial data are

$$\begin{pmatrix} \rho \\ u \\ P \end{pmatrix} = \begin{cases} (1,0,1)^T, & x < 0.5 \\ (0.125,0,0.1)^T, & x \geq 0.5. \end{cases}$$

Lax's Riemann problem: Initial data are

$$\begin{pmatrix} \rho \\ u \\ P \end{pmatrix} = \begin{cases} (0.445, 0.698, 3.528)^T, & x < 0.5 \\ (0.5, 0, 0.571)^T, & x \geq 0.5. \end{cases}$$

The numerical results using the component-wise convex ENO scheme are shown in Figure 2. There is a bit of smearing but no significant oscillations.

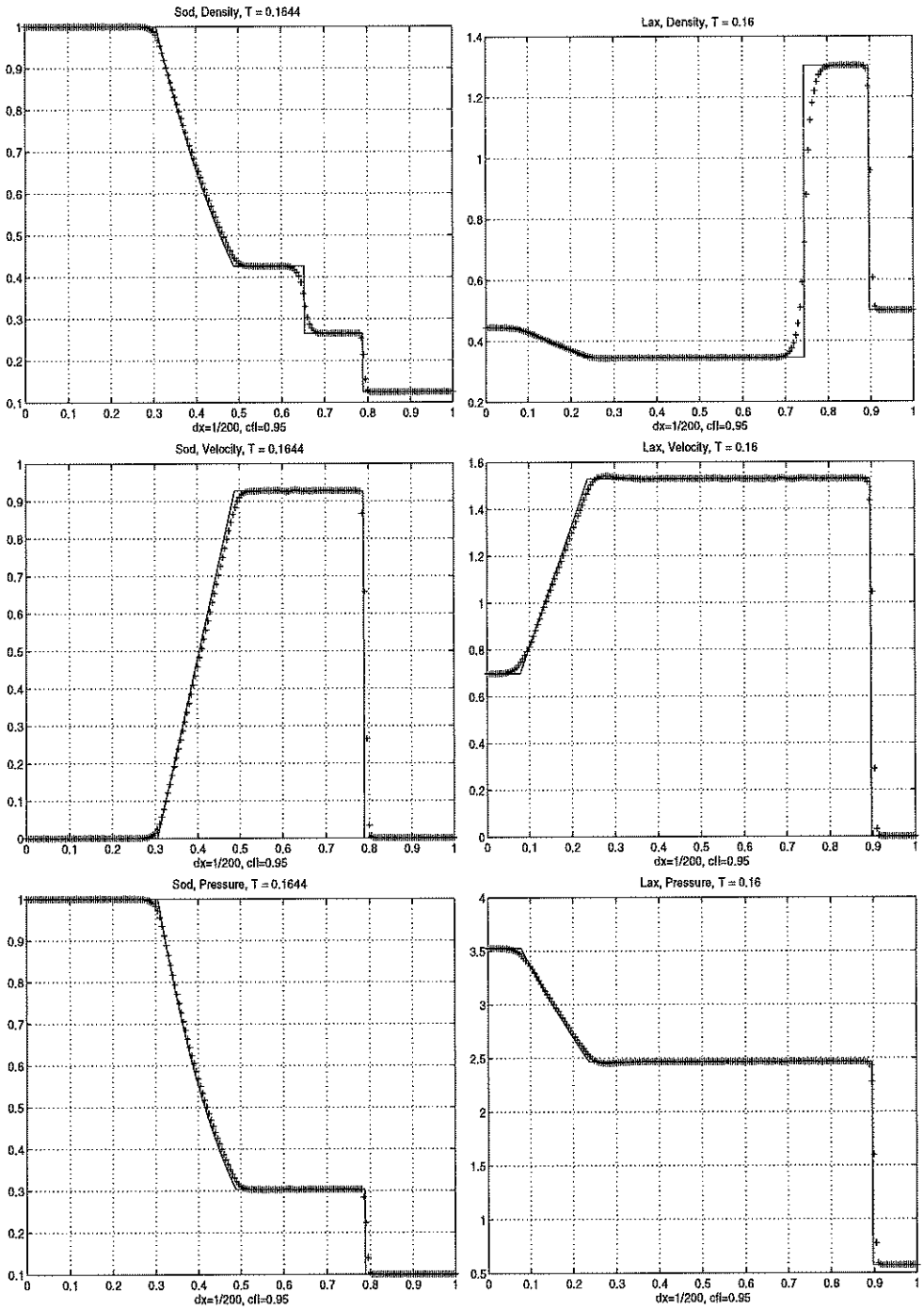

Figure 2: 3rd order component-wise CENO, minmod limiter, *left:* Sod problem and *right:* Lax problem

Example 3: Isolated Contact Discontinuity: Initial data are

$$\begin{pmatrix} \rho \\ u \\ P \end{pmatrix} = \begin{cases} (1,1,0.2)^T, & x < 0.5 \\ (2,1,0.2)^T, & x \geq 0.5. \end{cases}$$

It is gratifying to note that our component-wise convex ENO scheme yields a clean jump in ρ, with u and P remaining constant, Figure 3.

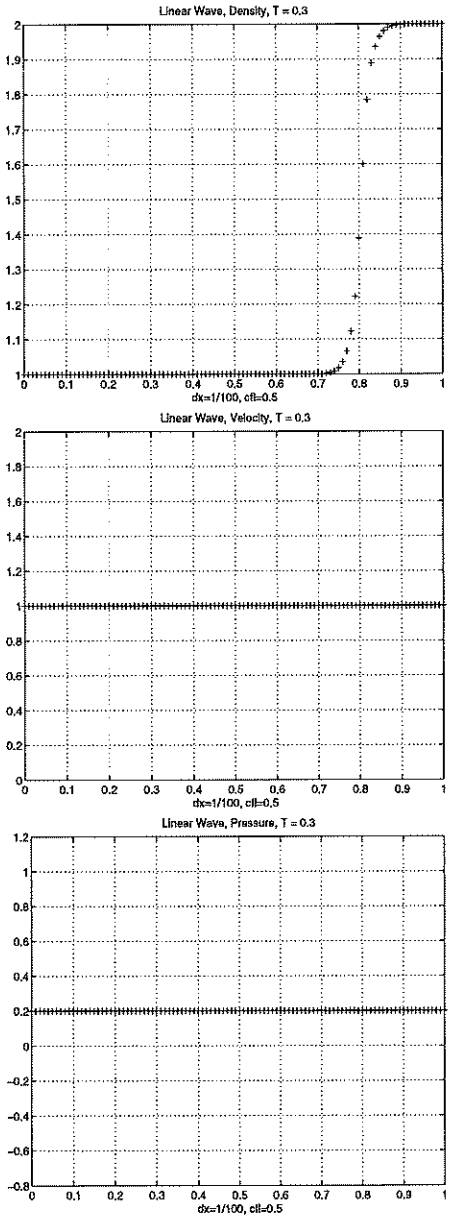

Figure 3: 3rd order component-wise CENO, minmod limiter, isolated contact discontinuity

Example 4: Shu-Osher sine wave hitting shock: Initial data are

$$\begin{pmatrix} \rho \\ u \\ P \end{pmatrix} = \begin{cases} (3.857143, 2.629369, 10.33333)^T, & x < 0.5 \\ (1 + 0.2 * \sin(50x - 25), 0, 1)^T, & x \geq 0.5. \end{cases}$$

The numerical results using the component-wise convex ENO scheme are displayed in Figure 4. Amusingly, they are very similar to those obtained by a TVD scheme using field-by-field limiting. This is a case where a different limiter for the second order scheme gives improved results. See Example 10 below.

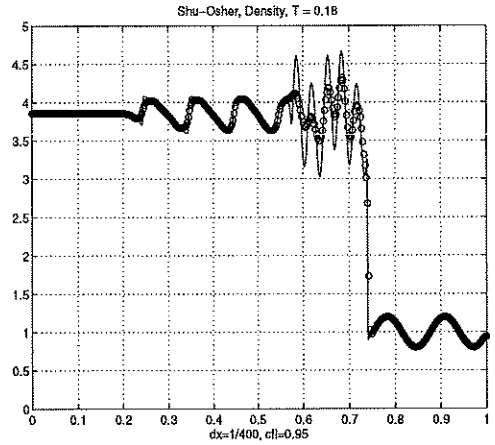

Figure 4: 3rd order component-wise CENO, minmod limiter, Shu-Osher problem

Example 5: Woodward-Colella problem: Initial data are

$$\begin{pmatrix} \rho \\ u \\ P \end{pmatrix} = \begin{cases} (1, 0, 1000)^T, & x < 0.1 \\ (1, 0, 0.01)^T, & 0.1 \leq x < 0.9 \\ (1, 0, 100)^T, & x \geq 0.9. \end{cases}$$

Reflecting boundary conditions are applied at both ends. The numerical results using the component-wise convex ENO scheme are displayed in Figures 5a-5b.

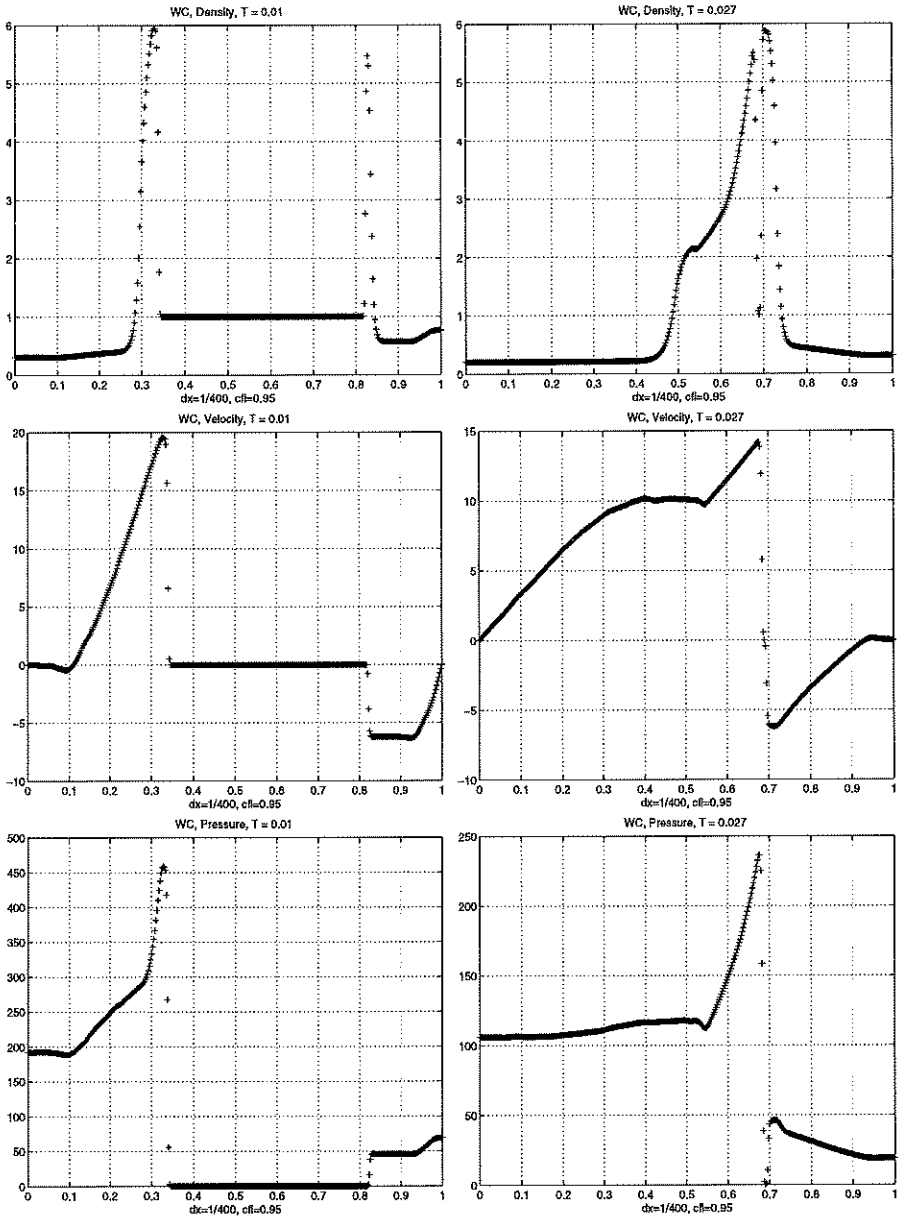

Figure 5a: 3rd order component-wise CENO, minmod limiter, Woodward Colella "Bang-bang" problem

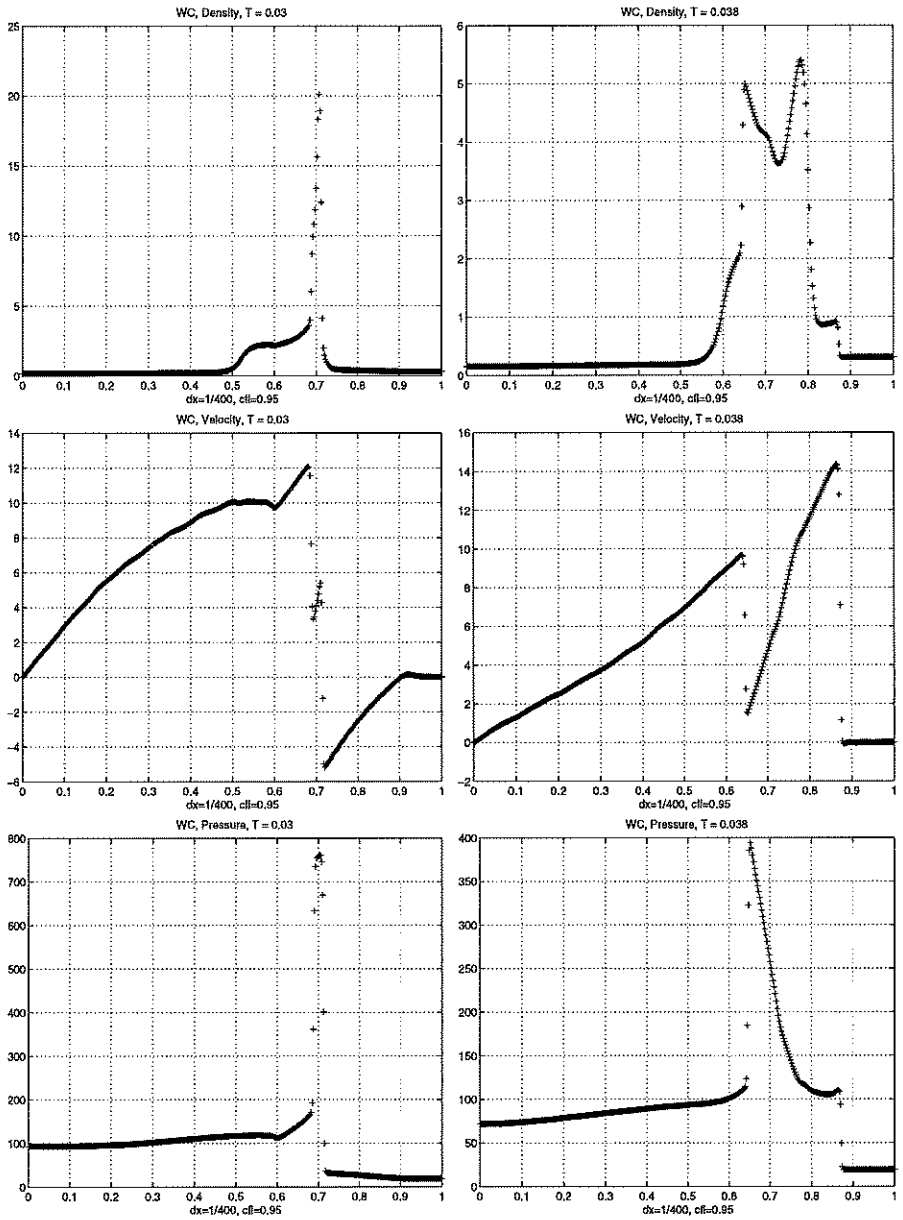

Figure 5b: same as **5a**

Example 6: Low density and internal energy Riemann problem: Initial data are

$$\begin{pmatrix} \rho \\ u \\ P \end{pmatrix} = \begin{cases} (1, -2, 0.4)^T, & x < 0.5 \\ (1, 2, 0.4)^T, & x \geq 0.5. \end{cases}$$

The results using component-wise convex ENO scheme are displayed in Figure 6. We note that the density and internal energy stay positive during the computational process. This is often not the case in the numerical approximation of this problem, in particular for high order accurate schemes.

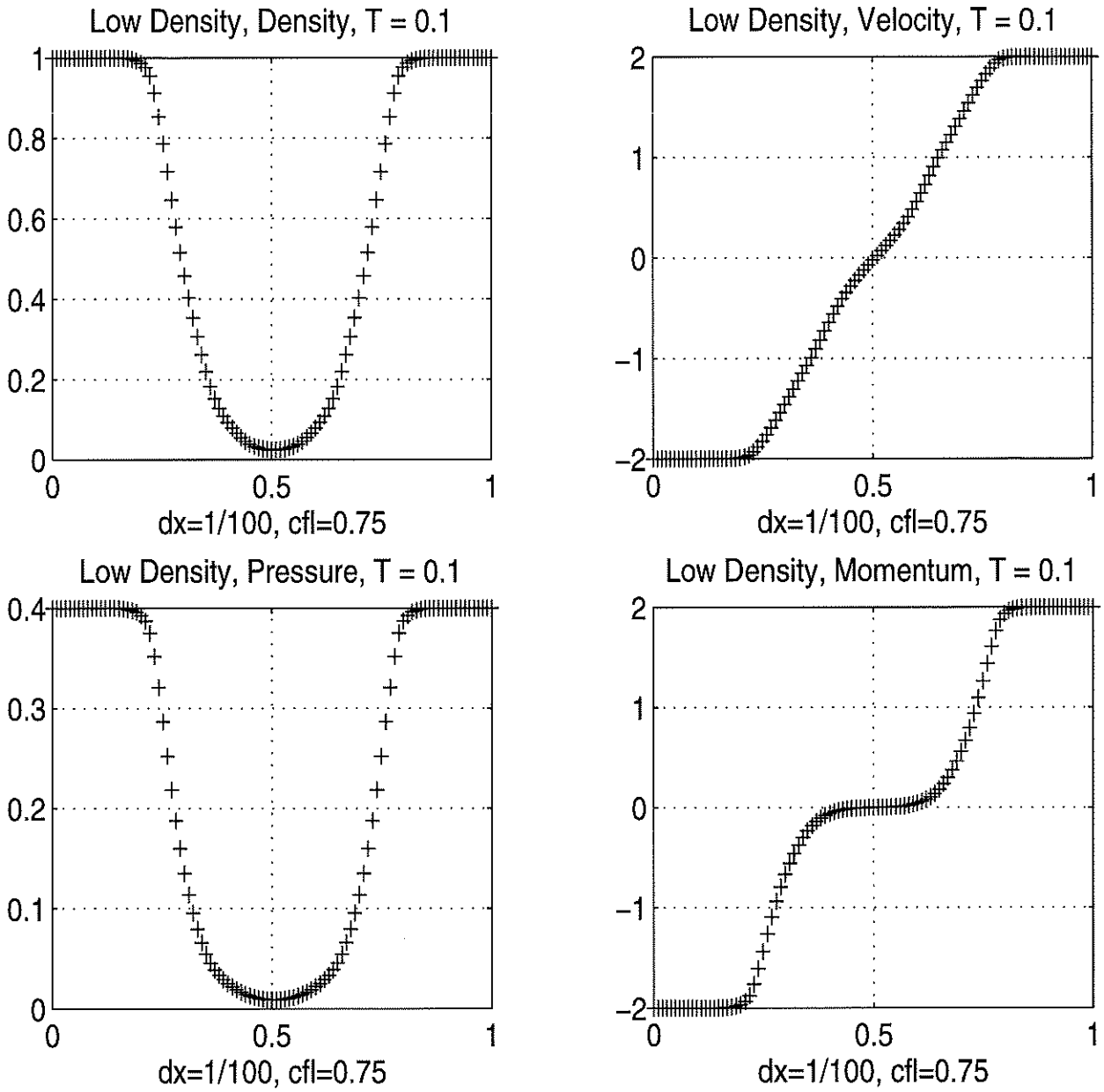

Figure 6: 3rd order component-wise CENO, minmod limiter, low density and internal energy Riemann problem

Now we test the accuracy of our third order schemes using the scalar linear problem

$$u_t + u_x = 0,$$

with initial data (i) $u(x,0) = sin(2\pi x)$, and (ii) $u(x,0) = sin^4(2\pi x)$. This problem is scalar and hence the component-wise and field-by-field versions are the same.The numerical results are presented in Table 1a-1d. This scalar convex ENO scheme achieves 3rd order accuracy in L_1.

Order of accuracy of 3rd order schemes

	$\nu_2 = 0.7$		$u(x,0) = sin^4(2\pi x)$	
number of points	error in L_∞	order in L_∞	error in L_1	order in L_1
20	0.130819466		0.055802221	
40	0.0222620419	2.55	0.00953868089	2.55
80	0.00720796238	1.63	0.00282921296	1.75
160	0.00264176553	1.45	0.000576823613	2.29
320	0.000787931253	1.75	0.000100661167	2.52
640	0.000166322806	2.24	1.3538874E-05	2.89
1280	4.86872147E-05	1.77	1.68882089E-06	3.00
2560	9.01723357E-06	2.43	2.26444779E-07	2.90
5120	3.5638503E-06	1.34	3.06878812E-08	2.88

Table 1a

	$\nu_2 = 0.5$		$u(x,0) = sin^4(2\pi x)$	
number of points	error in L_∞	order in L_∞	error in L_1	order in L_1
20	0.126124154		0.0530393427	
40	0.022317815	2.50	0.00930882882	2.51
80	0.00728537803	1.62	0.00233205651	2.00
160	0.0019271098	1.92	0.000375342064	2.64
320	0.000362526046	2.41	4.22597014E-05	3.15
640	6.54882088E-05	2.47	5.03039299E-06	3.07
1280	1.36249773E-05	2.27	6.25751426E-07	3.00
2560	2.94348851E-06	2.21	8.8273046E-08	2.83
5120	1.16642682E-08	7.98	2.40427676E-09	5.20

Table 1b

	$\nu_2 = 0.7$		$u(x,0) = sin(2\pi x)$	
number of points	error in L_∞	order in L_∞	error in L_1	order in L_1
20	0.00510279146		0.0031972175	
40	0.000616006547	3.05	0.000396621479	3.01
80	7.63561049E-05	3.01	4.91735717E-05	3.01
160	9.55266342E-06	3.00	6.11659336E-06	3.01
320	1.19432595E-06	3.00	7.62527964E-07	3.00
640	1.49299927E-07	3.00	9.51844875E-08	3.00
1280	1.86627503E-08	3.00	1.18896482E-08	3.00
2560	2.33285924E-09	3.00	1.48567948E-09	3.00
5120	2.91606295E-10	3.00	8.33867107E-11	4.16

Table 1c

	$\nu_2 = 0.5$		$u(x,0) = sin(2\pi x)$	
number of points	error in L_∞	order in L_∞	error in L_1	order in L_1
20	0.00506666592		0.00319841808	
40	0.000614441418	3.04	0.000396622292	3.01
80	7.63561049E-05	3.01	4.91735717E-05	3.01
160	9.55266342E-06	3.00	6.11659336E-06	3.01
320	1.19432595E-06	3.00	7.62527964E-07	3.00
640	1.49299927E-07	3.00	9.51844875E-08	3.00
1280	1.86627503E-08	3.00	1.18896482E-08	3.00
2560	2.33285924E-09	3.00	1.48567948E-09	3.00
5120	2.91606295E-10	3.00	8.33867107E-11	4.16

Table 1d

We consider two dimensional gamma law gas dynamics

$$U_t + F_1(U)_x + F_2(U)_y = 0,$$

where

$$\begin{aligned} U &= (\rho, m, n, E)^T \\ F_1(U) &= (m, \rho u^2 + P, \rho uv, u(E+P))^T \\ F_2(U) &= (n, \rho uv, \rho v^2 + P, v(E+P))^T \\ P &= (\gamma - 1)(E - \tfrac{1}{2}\rho(u^2 + v^2)) \\ m &= \rho u \\ n &= \rho v \end{aligned}$$

Example 7: Double Mach reflection:

A planar shock is incident on an oblique wedge at a 60° angle. The test problem involves a Mach 10 shock in air. The undisturbed air ahead of the shock has density of 1.4 and a pressure of 1. We use the boundary conditions

described in [21]. The flow at time $t = 0.2$ is plotted in Figure 7 with $\Delta x = \Delta y = \frac{1}{120}$, $\Delta t = \frac{1}{6} \times 10^{-4}$. The numerical results using the component-wise convex ENO scheme are plotted in 30 equally spaced contours.

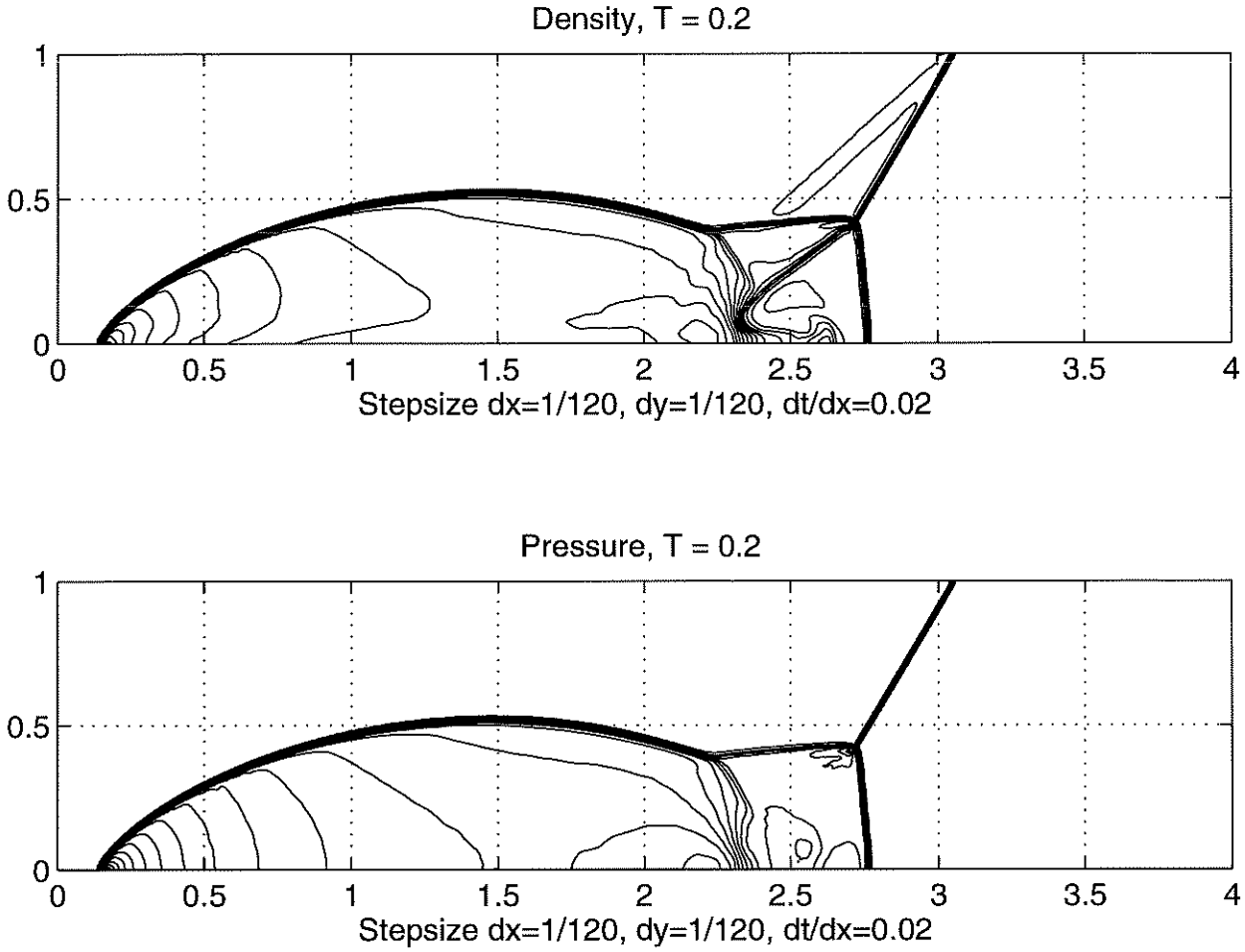

Figure 7: 3rd order component-wise CENO, minmod limiter, Double Mach reflection

Example 8: Engquist-Runborg example [3]:

$$\begin{pmatrix} q_1 \\ q_2 \end{pmatrix} + \begin{pmatrix} \frac{q_1^2}{\sqrt{q_1^2+q_2^2}} \\ \frac{q_1 * q_2}{\sqrt{q_1^2+q_2^2}} \end{pmatrix}_x + \begin{pmatrix} \frac{q_1 * q_2}{\sqrt{q_1^2+q_2^2}} \\ \frac{q_2^2}{\sqrt{q_1^2+q_2^2}} \end{pmatrix}_y = 0. \tag{38}$$

The system (38) represents a one-phase solution consisting of a single ray of strength $g(r,t) = \sqrt{q_1^2 + q_2^2}$, located at a distance r and an angle $\theta = arctan(q_2/q_1)$ relative to the single point source. The system (38) is *weakly* hyperbolic and hence field-by-field decomposition is impossible. The source is located at $(-0.2, 1)$ and the computational domain is the rectangle $0 \le x \le 1, 0 \le y \le 2$. The initial data are chosen to be zero (to avoid overflow we set $q_1 = q_2 = 10^{-12}$). We use inflow boundary conditions. In Table 2 we showed that our component-wise convex ENO scheme (using 4th order Runge-Kutta) works well with no loss of accuracy. It was reported in [10] that dimensional spitting caused a loss of accuracy for this difficult problem. We successfully used our dimension-by-dimension method, see Figure 8.

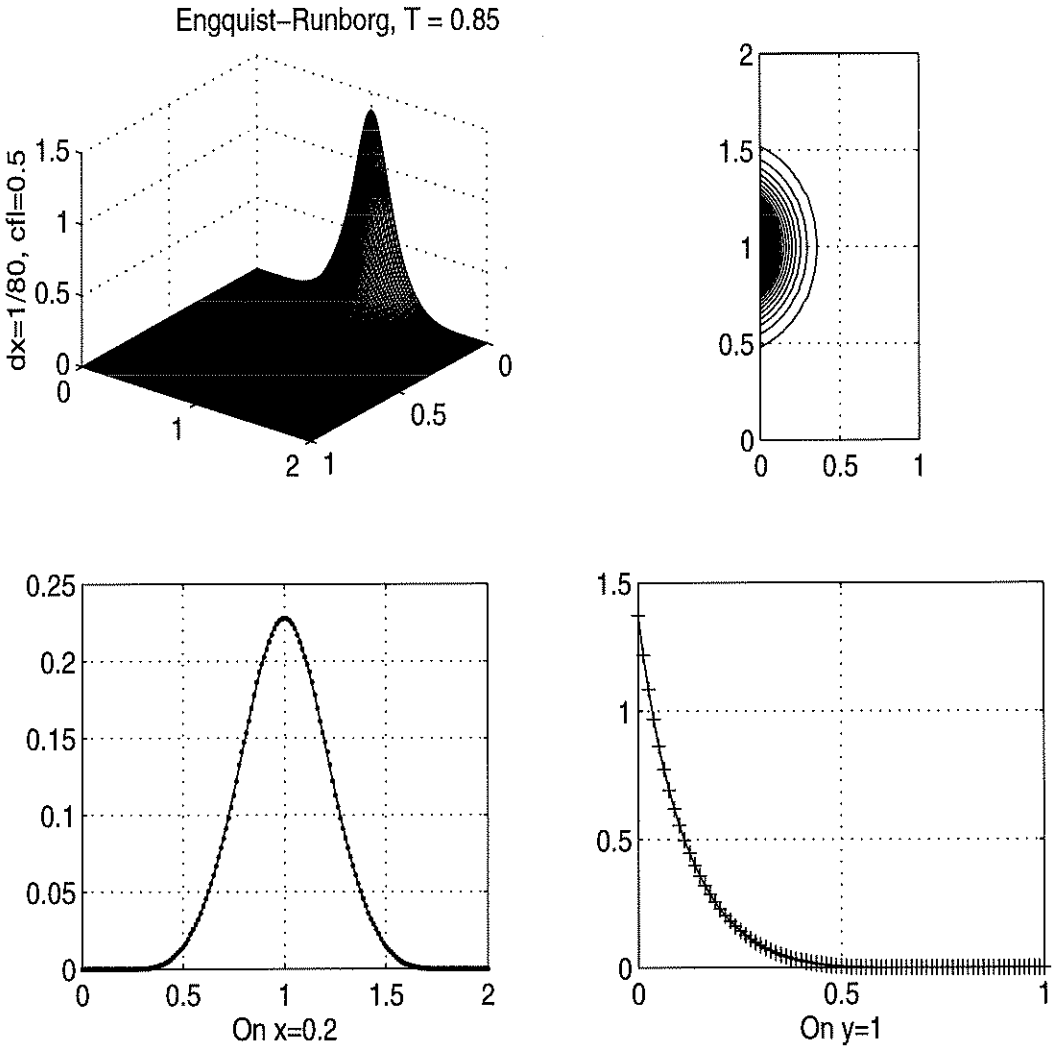

Figure 8: 3rd order component-wise CENO (4th order in time), minmod limiter, Engquist-Runborg weakly hyperbolic problem

number of points	error in L_∞	order in L_∞	error in L_1	order in L_1
20	0.0228		0.0012	
40	0.0100	1.19	3.0611E-4	1.97
80	0.0038	1.40	1.0348E-4	1.56
160	0.0017	1.16	2.5525E-5	2.02
320	1.7797E-4	3.26	2.8448E-6	3.17

Table 2

Example 9: Cavitation Shock for Water. A shock with a density jump travels down a tube of cavitated water with $\rho = 0.99$. A transition from the cavitated state to the water state occurs across the shock. Initial states are:

$$\begin{array}{lllll} \text{left (cavitated):} & \rho = 0.99, & p = 220.2725863533560, & u = 0, & x \leq 0.75 \\ \text{right (water):} & \rho = 1.001, & p = 24739399.54673034, & u = -524.027828, & x > 0.75 \end{array}$$

A uniform mesh is applied with 400 cells and a cell width of $\Delta x = 1/400$.

The problem terminates before the left boundary can influence the solution. Inflow condition are applied at the

right boundary. The Euler equation for water is

$$\begin{aligned} &\rho_t + m_x = 0 \\ &m_t + (m^2/\rho + P)_x = 0. \end{aligned}$$

The equation of state for water is chosen as

$$p(\rho) = \begin{cases} B\left((\rho/\rho_o)^\gamma - 1\right) + A & \text{if} \quad \rho > \rho_c \\ p_c & \text{otherwise,} \end{cases}$$

where $\gamma = 7.15$, $A = 10^6$, $B = 3.31 * 10^9$, $\rho_o = 1$, $\rho_c = 0.99995775$ and $p_c = 220.2725863533560$. Notice that (1) $p(\rho)$ only depends on ρ, hence conservation of energy is omitted in the Euler system. (2) When cavitated ($\rho \leq \rho_c$), the pressure is a constant, hence the sound speed c vanishes, and there is only one linearly independent eigenvector $(1, m/\rho)^T$. Therefore when water is cavitated the Euler system is weakly hyperbolic. Hence a strict field-by-field decomposition is impossible. Figure 9 shows the excellent numerical results of our 3rd order component-wise (using Lax-Friedrichs flux splitting) Convex ENO. There is no significant oscillation.

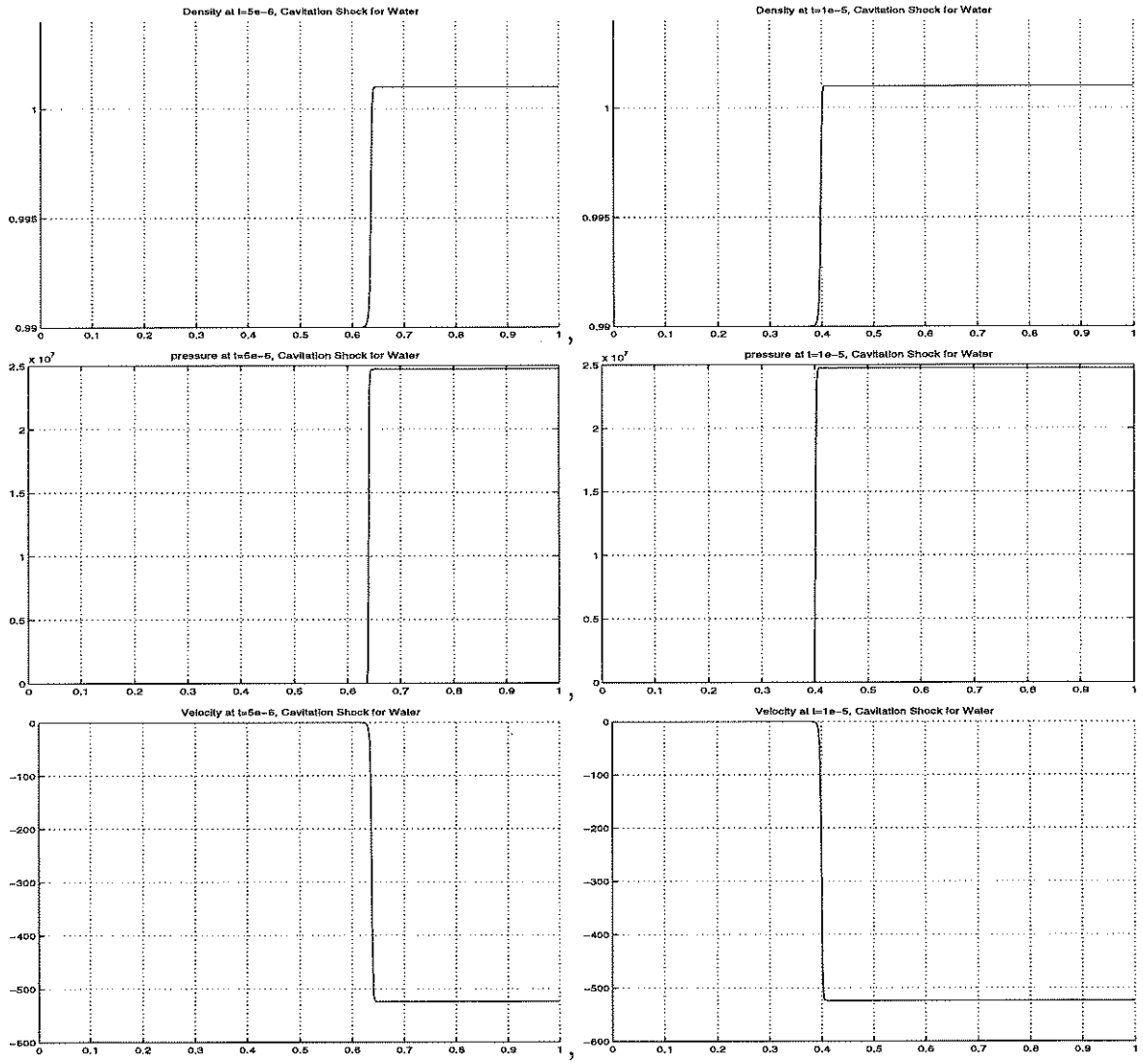

Figure 9: 3rd order component-wise CENO, minmod limiter, Cavitation Shock for Water

Example 10: Shu-Osher redone:
We repeat Example 4, this time using a new limiter

$$\varphi(r) = \max\left(0, \min(\frac{2r}{\nu}, 1 + (1+\nu)(r-1)/3, 2/(1-\nu))\right)$$

designed by Arora and Roe [1]. We chose $\nu = 0.75$ below. We base our component-wise convex ENO scheme on comparison with the $\hat{f}^{LLFar}_{j+\frac{1}{2}}$ flux. Figure 9 displays the results. They appear to be comparable (using much less effort) with those of third order field-by-field ENO scheme. However, this component-wise convex ENO scheme will yield somewhat oscillatory results for the other one dimensional test problems described here.

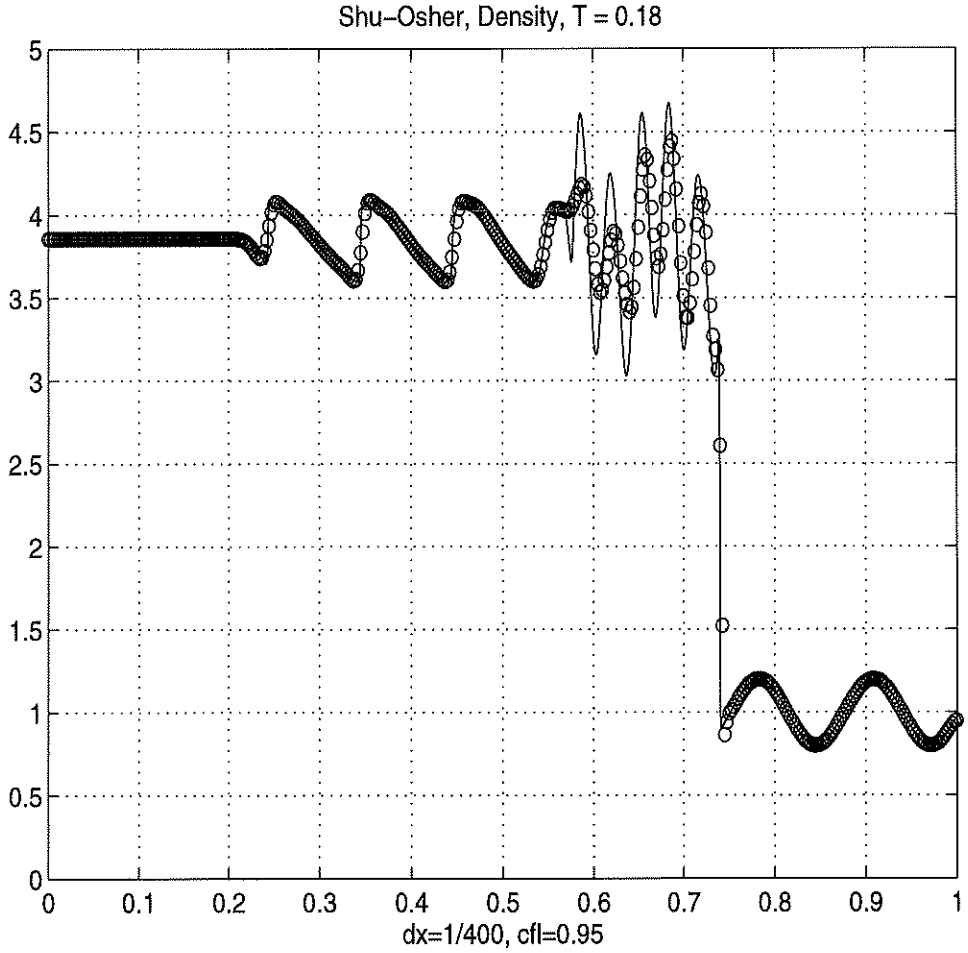

Figure 10: 3rd order component-wise CENO, Arora-Roe limiter, Shu-Osher problem

Thus, at this stage we recommend that $f^{LLFmm}_{j+\frac{1}{2}}$ be generally used for the component-wise methods – this is safe, but a bit smearing. Future research is needed along these lines.

Finally we show numerical results of our 3rd order accurate field-by-field convex ENO in Figures 11a-11f. We have found that the component-wise version of our convex ENO scheme is twice as fast as the field-by-field decomposition version in *each* dimension in all numerical experiments graphed below.

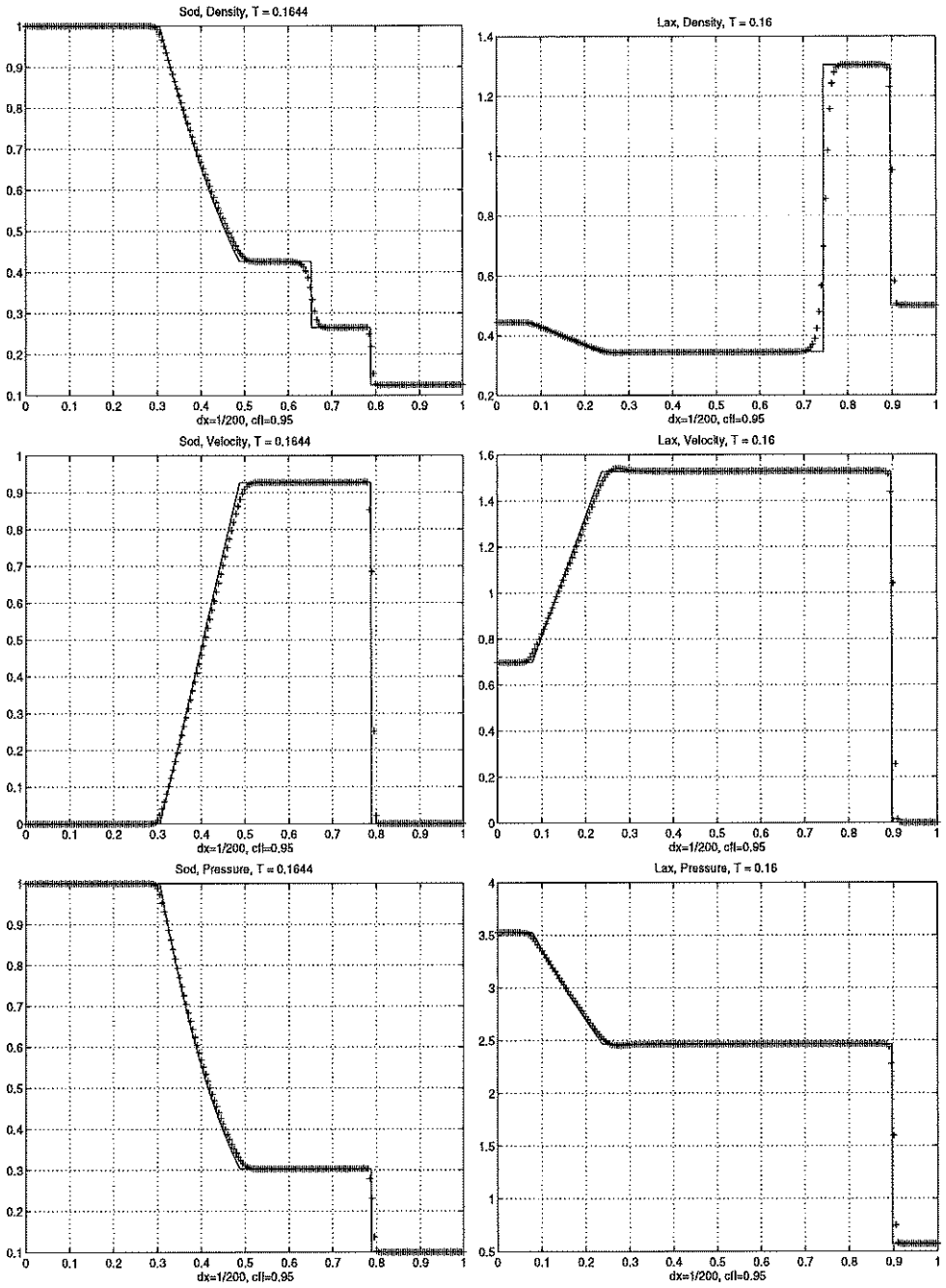

Figure 11a: 3rd order field-by-field CENO, minmod limiter, *left:* Sod problem, *right:* Lax problem

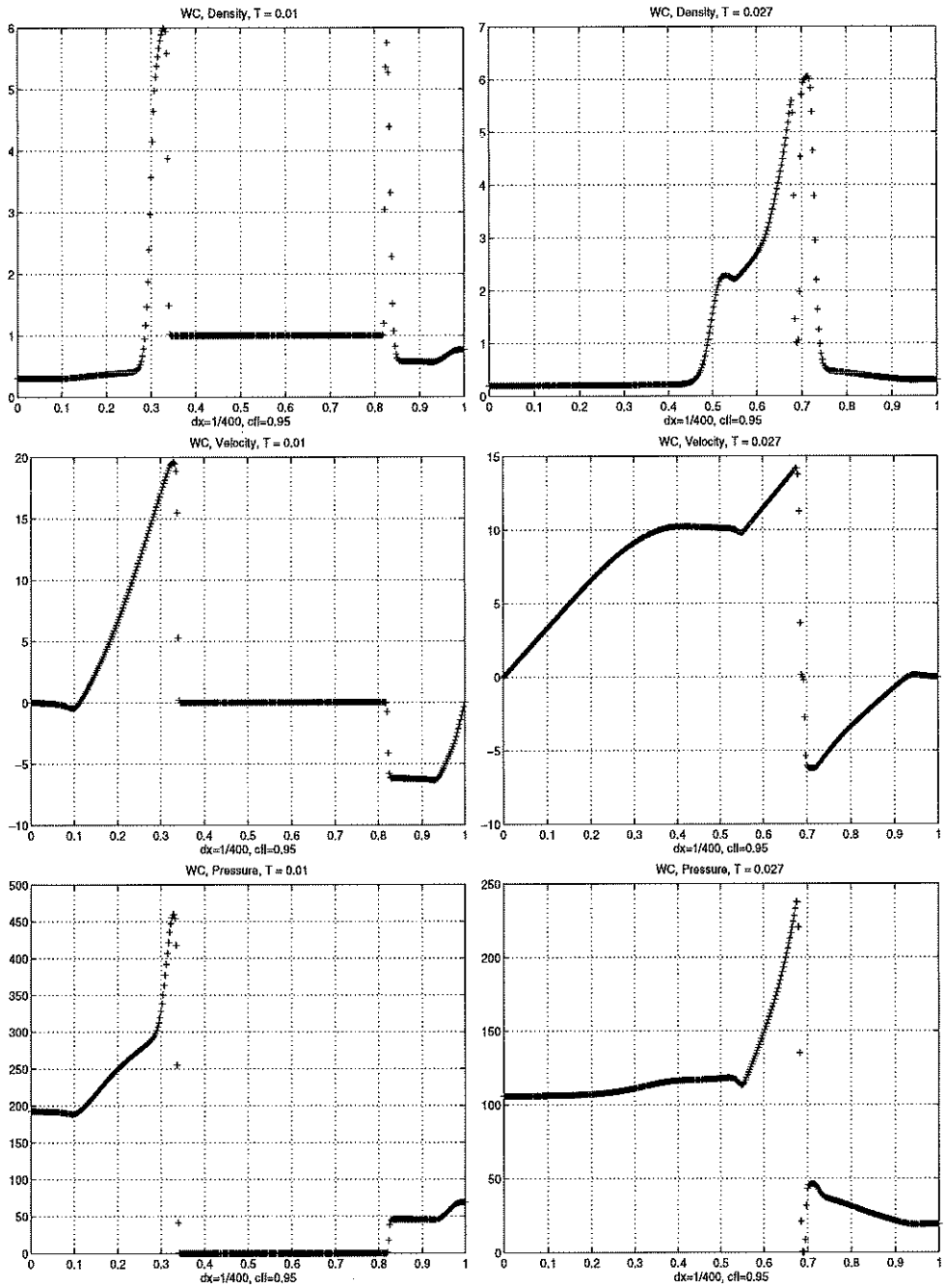

Figure 11b: 3rd order field-by-field CENO, minmod limiter, Woodward Colella "Bang-bang" problem

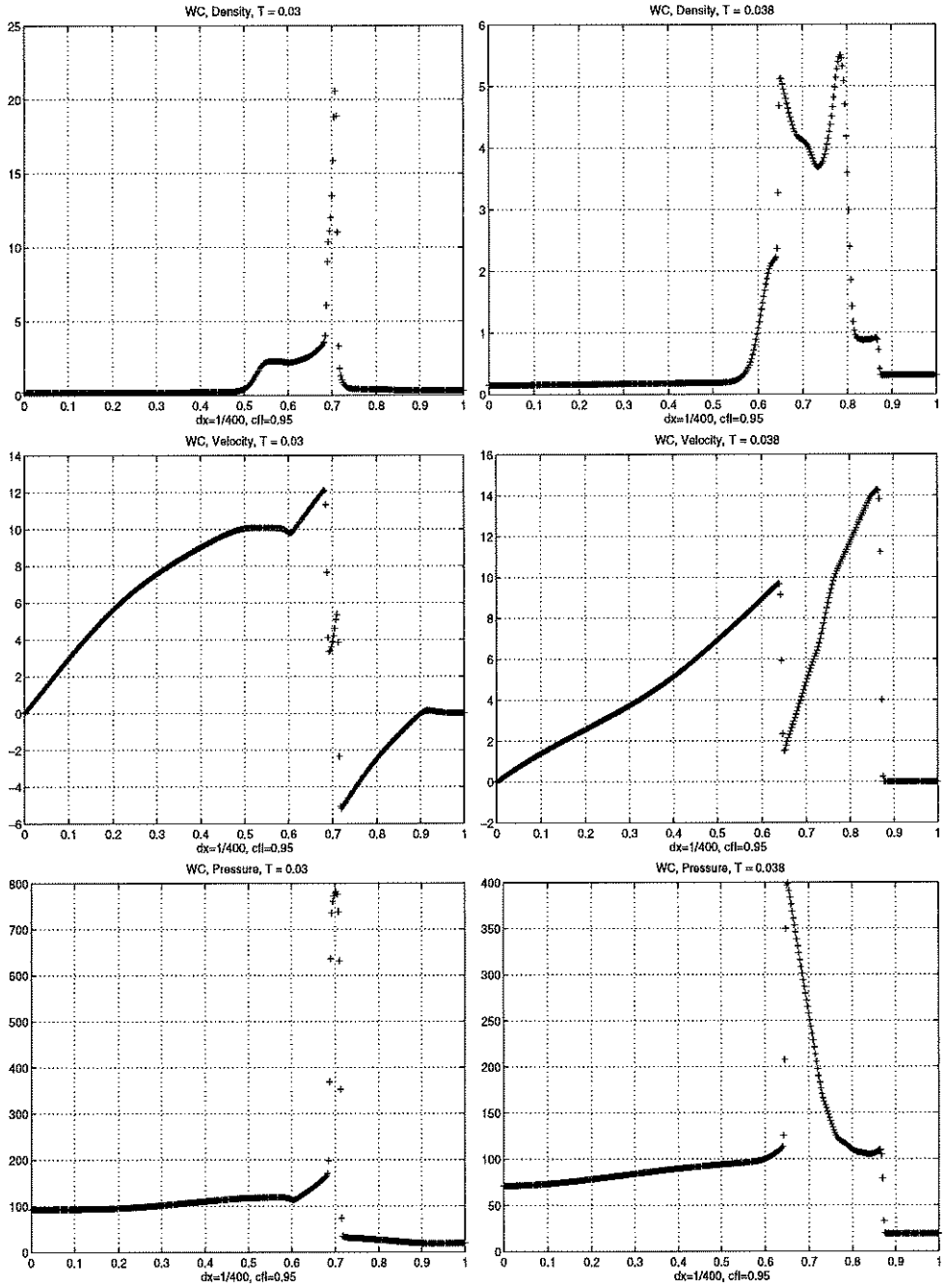

Figure 11c: 3rd order field-by-field CENO, minmod limiter, Woodward Colella "Bang-bang" problem

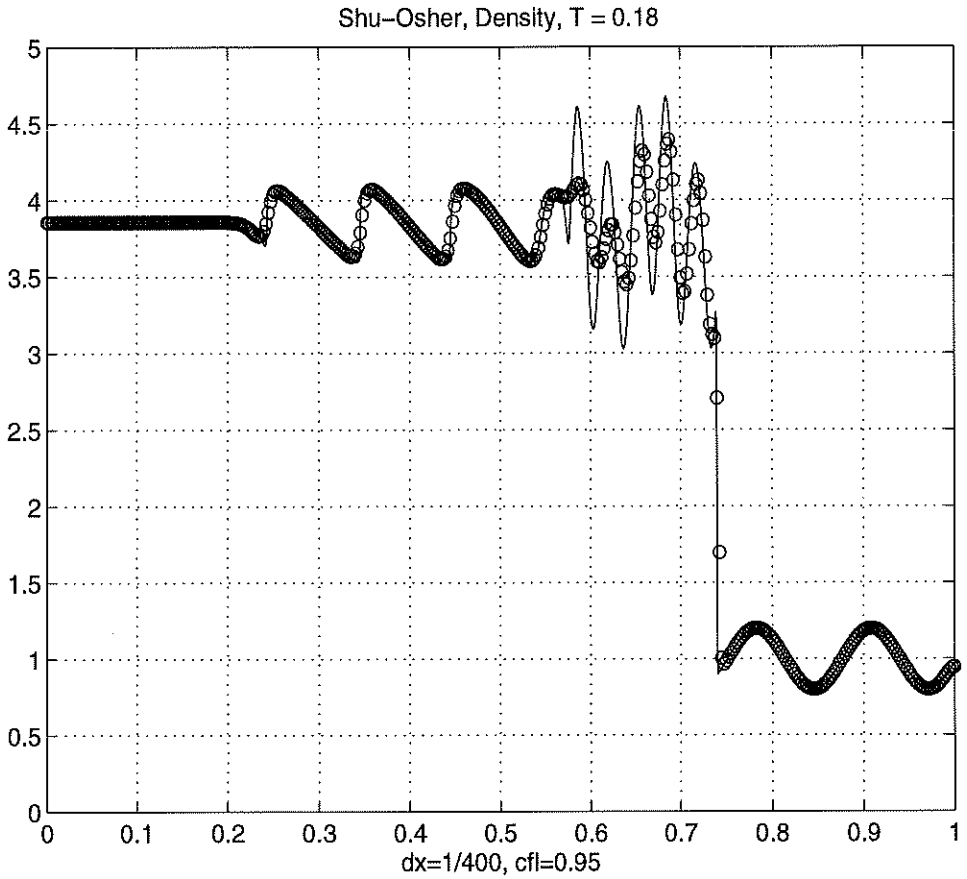

Figure 11d 3rd order field-by-field CENO, minmod limiter, Shu-Osher problem

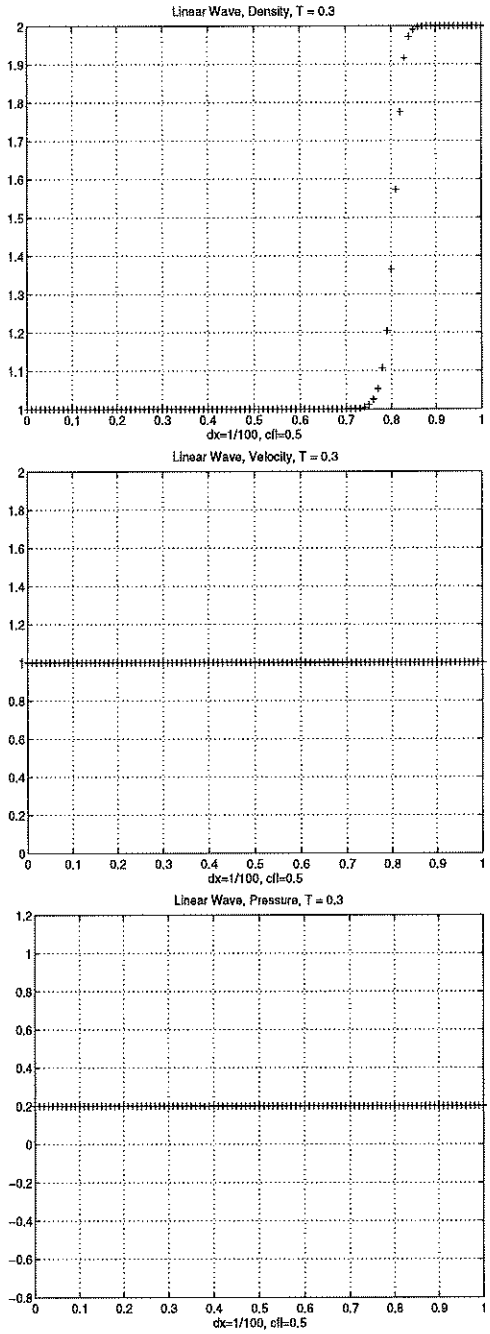

Figure 11e: 3rd order field-by-field CENO, minmod limiter, isolated contact discontinuity

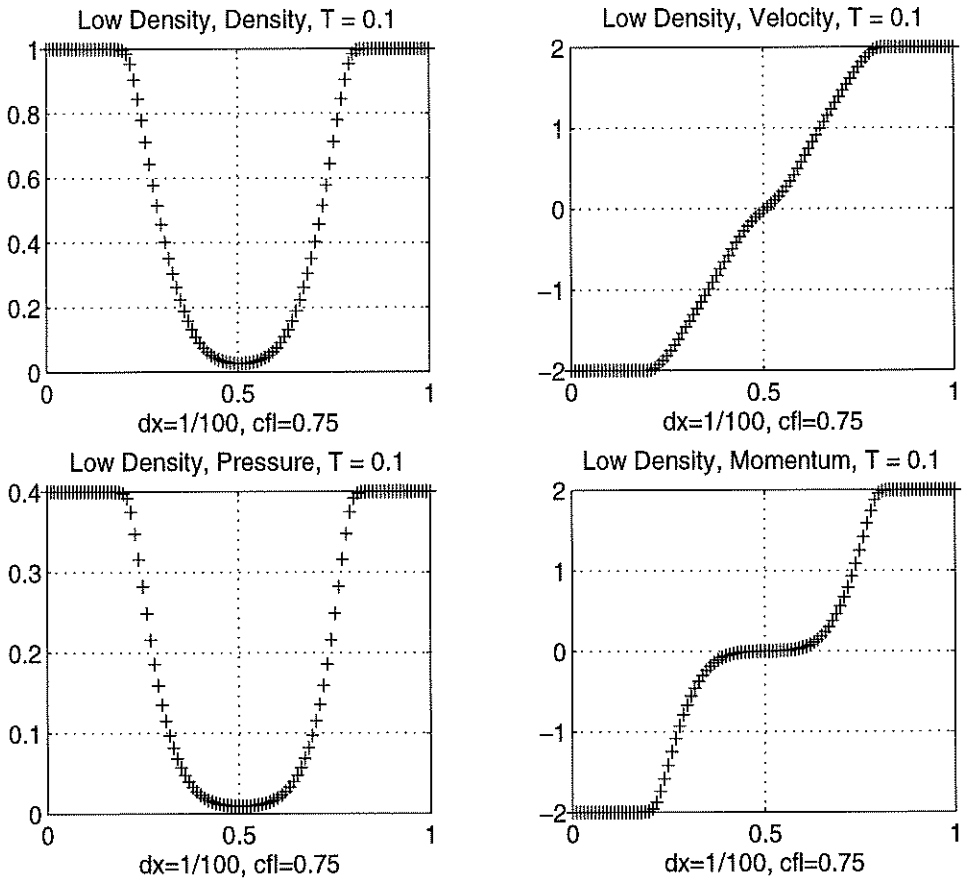

Figure 11f: 3rd order field-by-field CENO, minmod limiter, low density and internal energy Riemann problem

5 Conclusions

We have developed a very simple to implement and robust family of third order accurate convex ENO schemes. Their component-wise version do not use a field-by-field decomposition or staggered grids and still perform well. We have tested them over a wide range of, by now, standard canonical problems. The results show no significant oscillations. Furthermore the schemes preserve features quite well. See for example, the density at $t = 0.038$ in Figure 5b (component-wise calculations) as compared with the field-by-field results in Figure 11c. Resolving the peak on the right appears to be difficult for other component-wise schemes - see e.g. [10, 15]. The component-wise calculation was twice as fast in each dimension, which is typical.

We have extended the standard ENO interpolation procedure to a convex ENO decision process which appears to have some advantages of simplicity and performance over the traditional ENO methods.

The method appears to be easy to extend to arbitrarily high order of accuracy. We shall investigate this in the future.

References

[1] M. Arora and P.L. Roe, "A Well-Behaved TVD Limiter for High-Resolution Calculations of Unsteady Flow", *JCP* **132**, pp.3-11(1997).

[2] Hwajeong Choi and Jian-Guo Liu, "The Reconstruction of Upwind Fluxes for Conservation Laws,", submitted.

[3] B. Engquist and O. Runborg, "Multi-Phase Computations in Geometrical Optics", CAM Report 95-45 and *Comp. Appl. Math.*, v74, p175, (1996).

[4] A. Harten, "On a Class of High Resolution Total-Variation-Stable Finite-Difference Schemes," *SINUM*, **21**, No. 1, 1984, pp. 1-23.

[5] A. Harten, "High Resolution Schemes for Hyperbolic Conservation Laws," *JCP*, **49**, 1983, pp.357-393.

[6] A. Harten, B. Engquist, S. Osher and S. Chakravarthy, "Uniformly High Order Accurate Essentially Non-Oscillatory Schemes III," *JCP*, **71**, pp. 231-303, 1987; also ICASE Report No. 86-22, April 1986.

[7] A. Harten and S. Osher, "Uniformly High Order Accurate Non-oscillatory Scheme, I", *SINUM* **24**, 1982, pp.229-309.

[8] G.-S. Jiang, D.Levy, C.-T. Lin, S. Osher, and E.Tadmor, "High Resolution Non-Oscillatory Central Schemes with Non-staggered Grids for Hyperbolic Conservation Laws," *SINUM*, (to appear)

[9] G-S Jiang and C-W Shu, "Efficient Implementation of Weighted ENO Schemes", *JCP*, **126**, 1996, pp.202-228.

[10] G-S Jiang and E. Tadmor, "Non-oscillatory Central Schemes for Multidimensional Hyperbolic Conservation Laws", CAM Report 96-36.

[11] S. Jin and Z. Xin, "The Relaxing Schemes for Systems of Conservation Laws in Arbitrary Space Dimensions," *CPAM* **48**, 1995, pp.235-276.

[12] X.D. Liu and S. Osher, "Non-oscillatory High Order Accurate Self-Similar Maximum Principle Satisfying Shock Capturing Schemes, I", *SINUM* **33**, 1996.

[13] X.D. Liu and E. Tadmor, "Third Order Non-oscillatory Central Scheme for Hyperbolic Conservation Laws", *Numerische mathematik*, in press.

[14] E. Morano, R. Sanders, and M.-C. Druguet, "Multi-dimensional Dissipation for Upwind Schemes: Stablity and Applications to Gas Dynamics," (to appear).

[15] H. Nessyahu and E. Tadmor, "Non-oscillatory central differencing for hyperbolic conservation laws", *JCP* **87**, 1990, pp.408-448.

[16] S. Osher, "Riemann Solvers, the Entropy Condition and Difference Approximations," *SINUM*, **21**, 1984, pp.955-984.

[17] C.-W. Shu, "Numerical Experiments on the accuracy of ENO and Modified ENO Schemes," *J. Sci. Comput.* **5**, 1990, pp.127-150.

[18] C.-W. Shu and S. Osher, "Efficient Implementation of Essentially Non-oscillatory Shock-Capturing Schemes," *JCP* **77**, 1988, pp439-471.

[19] C.-W. Shu, Stanley Osher, "Efficient Implementation of Essentially Non-oscillatory Shock-Capturing Schemes, II," *JCP*, **83** , 1989, pp. 32-78.

[20] P.K. Sweby, "High Resolution Schemes Using Flux Limiters for Hyperbolic Conservation Laws" *SINUM*, **21**, No. 5, 1984, pp.995-1011.

[21] P. Woodward and P. Colella, "The Numerical Simulation of Two-Dimensional Fluid Flow with Strong Shocks," *JCP*, **54**, pp.115-173.